A "Conjugal" Consanguineous Family of Butadiynediyl-Derived Complexes: Synthesis and Electronic Ground States of Neutral, Radical Cationic, and Dicationic Iron/Rhenium C_4 Species

Frédéric Paul,[†] Wayne E. Meyer,[‡] Loic Toupet,[§] Haijun Jiao,[⊥] John A. Gladysz,*[,‡,⊥] and Claude Lapinte*[,†]

Contribution from the UMR CNRS 6509, Organometalliques et Catalyse, University de Rennes I, Campus de Beaulieu, 35042 Rennes, France, Department of Chemistry, University of Utah, Salt Lake City, Utah 84112, UMR CNRS 6626, Groupe Matière Condensée et Materiaux, University de Rennes I, Campus de Beaulieu, 35042 Rennes, France, and the Institut für Organische Chemie, Friedrich-Alexander Universität Erlangen-Nürnberg, Henkestrasse 42, 91054 Erlangen, Germany

Received March 29, 2000

Abstract: The reaction of (η^5-C_5Me_5)Re(NO)(PPh_3)(C≡CC≡CSiMe_3) and (η^5-C_5Me_5)Fe(η^2-dppe)(Cl) with KF, KPF_6, and 18-crown-6 in MeOH/THF gives the heterobimetallic butadiynediyl complex (η^5-C_5Me_5)Re(NO)(PPh_3)(C≡CC≡C)(η^2-dppe)Fe(η^5-C_5Me_5) (**9**, 65%). This can be oxidized with [(η^5-C_5H_5)$_2$Fe]$^+$ PF_6^- to the isolable radical cation **9**$^+$ PF_6^- and dication **9**$^{2+}$ 2PF_6^-, which constitute the first conjugal consanguineous family of C_x complexes. The crystal structure of **9** is determined, and **9**$^{n+}$ *n*PF_6^- are characterized in detail by cyclic voltammetry (CV) and IR, NMR, near-IR, ESR, and ^{57}Fe Mössbauer spectroscopies. The bond lengths/angles suggest some bridge polarization in **9**, and CV data show that the iron and rhenium endgroups communicate strongly. The odd electron in **9**$^+$ PF_6^- is delocalized between the endgroups. In **9**$^{2+}$ 2PF_6^-, both electronic and magnetic interactions are found between remote unpaired spins on the rhenium and iron endgroups. This antiferromagnetic coupling stabilizes the singlet cumulenic over the triplet butadiynediyl state. At room temperature, however, both isomers of **9**$^{2+}$ 2PF_6^- are simultaneously present. Data are carefully compared to those of the analogous consanguineous diiron and dirhenium complexes.

Introduction

The rapidly growing interest in molecular electronics is evidenced by increasing reports of new nanoscale-sized "smart" organic or organometallic molecules with tailor-made properties such as recognition or switching ability.[1−10] A prerequisite to the development of supermolecules incorporating these devices is efficient and modular electron conveyors. Several wire-like bimetallic polyynediyl complexes, reported recently by us and others,[11−16] constitute promising building blocks in this respect. Two representative examples are the homobimetallic butadiynediyl complexes **1a**,**b**, which feature the 17-valence-electron chiral rhenium and achiral iron endgroups (η^5-C_5Me_5)Re(NO)(PPh_3)[11] and (η^5-C_5Me_5)Fe(η^2-dppe),[12] respectively. These provide particularly interesting models for studies since they can be transformed into stable, isolable, and "consanguineous"[11] single- and double-oxidized states, **1a**,**b**$^+$ X^- and **1a**,**b**$^{2+}$ 2X^-.

[†] UMR CNRS 6509 Organometalliques et Catalyse.
[‡] University of Utah (former address).
[§] UMR CNRS 6626 Groupe Matière Condensée et Matériaux.
[⊥] Friedrich-Alexander Universität Erlangen-Nürnberg.

(1) Ziessel, R.; Hissler, M.; Ghayoury, E.; Harriman, A. *Coord. Chem. Rev.* **1999**, *178−180*, 1251−1298. (b) Ziessel, R. *Synthesis* **1999**, 1839−1865.
(2) Martin, R. E.; Diederich, F. *Angew. Chem. Int. Ed.* **1999**, *38*, 1350−1377; *Angew. Chem.* **1999**, *111*, 1440−1469.
(3) Schwab, P. H. F.; Levin, M. D.; Michl, J. *Chem. Rev.* **1999**, *99*, 1863−1933.
(4) Creager, S.; Yu, C. J.; Bamdad, C.; O'Connor, S.; MacLean, T.; Lam, E.; Chong, Y.; Olsen, G. T.; Luo, J.; Gozin, M.; Kayyem, J. F. *J. Am. Chem. Soc.* **1999**, *121*, 1059−1064.
(5) Paul, F.; Lapinte, C. *Coord. Chem. Rev.* **1998**, *178/180*, 427−505.
(6) Swager, T. M. *Acc. Chem. Res.* **1998**, *31*, 201−207.
(7) (a) Ward, M. D. *Chem. Soc. Rev.* **1997**, *26*, 365−375. (b) Ward, M. D. *Chem. Ind.* **1996**, *15*, 568−573. (c) Ward, M. D. *Chem. Soc. Rev.* **1995**, *24*, 121−134. (d) McCleverty, J. A.; Ward, M. D. *Acc. Chem. Res.* **1998**, *31*, 842−851.
(8) Barigelletti, F.; Flamigni, L.; Collin, J.-P.; Sauvage, J.-P. *Chem. Commun.* **1997**, 333−338.
(9) (a) Harriman, A.; Sauvage, J.-P. *Chem. Soc. Rev.* **1996**, 41−48. (b) Sauvage, J.-P.; Collin, J.-P.; Chambron, J.-C.; Guillerez, S.; Coudret, C. *Chem. Rev.* **1994**, *94*, 993−1019.
(10) Grosshenny, V.; Harriman, A.; Hissler, M.; Ziessel, R. *Platinum Met. Rev.* **1996**, *40*, 26−35 and 72−77.
(11) Brady, M.; Weng, W.; Zhou, Y.; Seyler, J. W.; Amoroso, A. J.; Arif, A. M.; Böhme, M.; Frenking, G.; Gladysz, J. A. *J. Am. Chem. Soc.* **1997**, *119*, 775−788.
(12) (a) Le Narvor, N.; Toupet, L.; Lapinte, C. *J. Am. Chem. Soc.* **1995**, *117*, 7129−7138. (b) Le Narvor, N.; Lapinte, C. C. R. *Acad. Sci.* **1998**, T1, Ser. IIc, 745−749.
(13) (a) Bruce, M. I. *Coord. Chem. Rev.* **1997**, *166*, 91−119. (b) Bruce, M. I.; Denisovich, L. I.; Low, P. J.; Peregudova, S. M.; Ustynyuk, N. A. *Mendeleev Commun.* **1996**, 200−201. (c) Bruce, M. I.; Hinterding, P.; Tiekink, E. R. T.; Skelton, B. A.; White, A. H. *J. Organomet. Chem.* **1993**, *450*, 209−218. (d) Bruce, M. I.; Low, P. J.; Costuas, K.; Halet, J.-F.; Best, S. P.; Heath, G. A. *J. Am. Chem. Soc.* **2000**, *122*, 1949−1962.
(14) (a) Coat, F.; Lapinte, C. *Organometallics* **1996**, *15*, 477−479. (b) Guillemot, M.; Toupet, L.; Lapinte, C. *Organometallics* **1998**, *17*, 1928−1930.
(15) Dembinski, R.; Bartik, T.; Bartik, B.; Jaeger, M.; Gladysz, J. A. *J. Am. Chem. Soc.* **2000**, *122*, 810−822.
(16) For crystallographically characterized symmetrical butadiynediyl complexes, see refs 13, 14b, and the following: (a) Kheradmandan, S.; Heinze, K.; Schmalle, H. W.; Berke, H. *Angew. Chem. Int. Ed.* **1999**, *34*, 2270−2273; *Angew. Chem.* **1999**, *111*, 2412−2415. (b) Akita, M.; Chung, M.-C.; Sakurai, A.; Sugimoto, S.; Terada, M.; Tanaka, M.; Moro-oka, Y. *Organometallics* **1997**, *16*, 4882−4888. (c) Yam, V. W.-W.; Lau, V. C.-Y.; Cheung, K.-K. *Organometallics* **1996**, *15*, 1740−1744. (d) Gevert, O.; Wolf, J.; Werner, H. *Organometallics* **1996**, *15*, 2806−2809. (e) Ren, T.; Zou, G.; Alvarez, J. C. *Chem. Commun.* **2000**, 1197−1198.

10.1021/ja0011055 CCC: $19.00 © 2000 American Chemical Society
Published on Web 09/13/2000

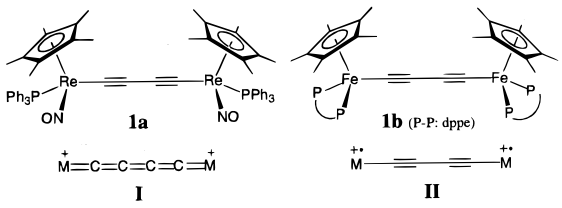

Much information about the impressive electron transfer capabilities of wire-like sp carbon chains has been extracted by the study of mixed valence (MV) states of such complexes. Both the iron and rhenium endgroups have proved particularly effective, offering several complementary probes. Spectroscopic studies indicate that oxidation induces a progressive change in the electronic structure of the bridge, but many properties are influenced by the metal termini. This is clearly illustrated by the C_4 dirhenium and diiron dications. A cumulenic structure (**I**) is found for $\mathbf{1a}^{2+}$ $2PF_6^-$, which has a singlet ground state.[11] However, a spin equilibrium is observed for $\mathbf{1b}^{2+}$ $2PF_6^-$. This compound also has a singlet ground state, but the separation between singlet and triplet states is so weak ($J = -18$ cm^{-1}) that both are thermally populated even at liquid nitrogen temperature.[12b] As a butadiynediyl structure (**II**) is expected for the triplet state, the C_4 ligand mediates both energetic and magnetic communication between the metal termini.[12a]

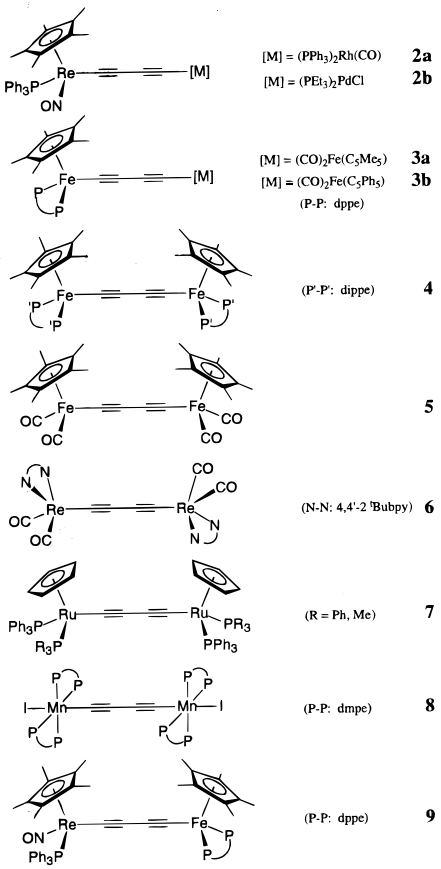

For similar reasons, *nonsymmetrical* or "conjugal"[11] complexes with different endgroups have also been independently studied by our groups, viz., **2a**,**b**[17] and **3a**,**b**.[18] We found that the singly oxidized mixed valence states of the conjugal complexes have less delocalized electronic holes than their symmetrical counterparts (e.g., $\mathbf{3a}^+$ PF_6^- vs $\mathbf{1b}^+$ PF_6^-), despite the highly polarized carbon bridges. However, the poor stability of the oxidized forms of many of these first generation systems (e.g., $\mathbf{2b}^+$ PF_6^-, $\mathbf{3a}$,$\mathbf{b}^{2+}$ $2PF_6^-$) hindered detailed studies. This further illustrates the effect of the metal termini upon the physical and chemical properties of such complexes.

Scheme 1. Synthesis of the Conjugal C_4 Complex **9**

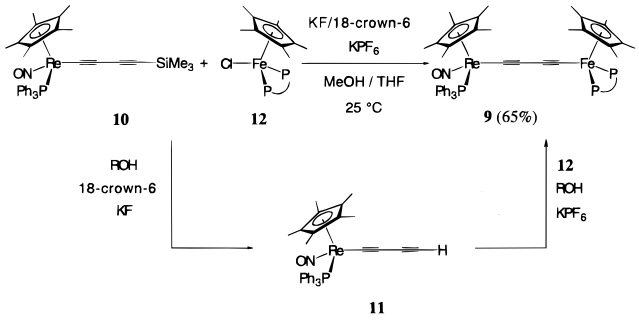

The number of stable oxidation states strongly depends on the terminal ends as shown by the comparison between the complexes **4**,[14b] **5**,[16b] and **6**.[16c] Another example of a C_4-bridged complex is the diruthenium compound **7**,[13d] which undergoes four stepwise single-electron oxidations, as assayed by cyclic voltammetry. This novel series of five oxidation states includes the formal mixed valence states Ru(II)−Ru(III) and Ru(III)−Ru(IV). Interestingly, the dimanganese complex **8**[16a] has a paramagnetic triplet ground state, in contrast to the other neutral complexes above. This compound is derived from the 16-valence-electron Mn(η^2-dmpe)$_2$(I) endgroup, and is easily oxidized to the corresponding radical cation and diamagnetic dication. Structural and IR data indicate that the triplet ground state of **8** has alternating C−C and C≡C bonds, and the diamagnetic singlet dication is cumulenic.

To best study and analyze the effects and interplay of unlike endgroups in such systems, we decided to investigate the title series of conjugal consanguineous complexes $\mathbf{9}^{n+}$ nPF_6^-, which feature the iron and rhenium endgroups (η^5-C_5Me_5)Fe(η^2-dppe) and (η^5-C_5Me_5)Re(NO)(PPh_3) that render such a broad range of oxidation states isolable with $\mathbf{1a,b}^{n+}$ nPF_6^-. In this paper, we describe the synthesis and detailed structural, spectroscopic, and electronic characterization of **9**, the radical cation $\mathbf{9}^+$ PF_6^-, and the dication $\mathbf{9}^{2+}$ $2PF_6^-$. Their properties are carefully analyzed with respect to $\mathbf{1a,b}^{n+}$ nPF_6^-. These data provide important benchmarks for future studies of conjugal C_x complexes, such as analogues with longer carbon chains, polymetallic endgroups, and/or protective microenvironments.

Results

1. Synthesis and Characterization of 9. As outlined in Scheme 1, **9** was synthesized via a protocol similar to one developed for related diiron complexes.[18] The trimethylsilylbutadiynyl complex **10**, which is stable as a solid for extended periods, was transformed by a fluoride-ion-containing recipe (KF, KPF_6, 18-crown-6)[19] to the butadiynyl complex **11**, which then coupled with the iron chloride **12**. Such desilylations are well-known in organic reactions, but are less used in organometallic synthesis.[20] NMR monitoring showed that **12** was consumed after 24 h. Workup gave **9** as a spectroscopically

(17) Weng, W. Q.; Bartik, T.; Brady, M.; Bartik, B.; Ramsden, J. A.; Arif, A. M.; Gladysz, J. A. *J. Am. Chem. Soc.* **1995**, *117*, 11922−11931.

(18) Coat, F.; Guillevic, M.-A.; Toupet, L.; Paul, F.; Lapinte, C. *Organometallics* **1997**, *16*, 5988−5998.

(19) No reaction was observed in the absence of 18-crown-6, a good binder for potassium ions that would be expected to enhance the nucleophilicity of the KF. Optimum yields were obtained with roughly 2 equiv, possibly due to the presence of KPF_6.

Table 1. Selected ^{1}H NMR Chemical Shifts (ppm) for C_4 Complexes with Iron and/or Rhenium Endgroups

compd	η^5-$C_5(CH_3)_5$	C_6H_5	solvent	ref
9	1.76 (Re); 1.50 (Fe)	7.3−7.0; 8.2−7.8	C_6D_6	this work
9^{2+} 2PF_6^-	2.25 (Re); 1.20 (Fe)	7.60−6.50	CD_2Cl_2	this work
1a	1.68 (Re)	7.56−7.48	THF-d_8	11
1a^{2+} 2PF_6^-	2.03 (Re)	7.63−7.25	CD_2Cl_2	11
1b	1.55 (Fe)	8.16−7.00	C_6D_6	12a
1b^{2+} 2PF_6^-	−6.03 (Fe)	9.6−6.2	CD_2Cl_2	12a

pure orange powder in 65% yield. A similar coupling could be effected with **11** and **12**, but overall yields for this two-step sequence were lower.

A FAB mass spectrum of **9** showed the expected parent ion, but the microanalysis was not very satisfactory. Cube-shaped crystals, obtained from CH_2Cl_2/pentane, gave a microanalysis very close to that expected for the solvate **9**·CH_2Cl_2. NMR spectra were severely broadened unless freshly crystallized samples and carefully deoxygenated solvents were used. This problem was much more severe than with FeC≡CC≡CFe systems studied previously. The generally broad lines can be attributed to fast electron exchange with traces of an oxidized paramagnetic compound. This phenomenon has abundant precedent.[21,22]

At −80 °C, the ^{31}P NMR spectrum showed two signals in a 2:1 ratio.[22] The ^{1}H NMR spectrum (−80 °C) confirmed the presence of the solvate, and showed two $C_5(CH_3)_5$ signals, with the upfield one always broader. This was assigned, by analogy to the chemical shift trend in **1a** and **1b** (Table 1), to the iron-bound ligand. Unfortunately, the ^{13}C signals of the C_4 ligand could not be definitively detected. Such resonances are always difficult to observe, and **9** presents an even greater challenge due to the potential for coupling to three inequivalent phosphorus nuclei, and a poor low-temperature solubility.

The IR spectrum of **9** exhibits a strong ν_{NO} band at 1620 cm^{-1} and two medium/weak $\nu_{C\equiv C}$ bands at 2058 and 1956 cm^{-1} (Table 2). The latter absorptions are consistent with a slight polarization of the carbon bridge, as previously observed with **3a**,**b**. The ν_{NO} band is shifted relative to those of monorhenium complexes **10** and **11** (Table 2), analogously to **1a**.[23] Also, the $\nu_{C\equiv C}$ bands in **9** are shifted relative to those of **10** and **11** as well as the monoiron complex (η^5-C_5Me_5)Fe(η^2-dppe)(C≡CC≡CSiMe_3) (**13**). This indicates that the iron endgroup is more electron releasing than trimethylsilyl. Furthermore, **9** exhibits a shoulder at 2093−2095 cm^{-1}, both in solution and solid state (crystals and powders). This might be due to the Fermi coupling with another vibrational mode involving atoms adjacent to the triple bonds, as suggested for mononuclear iron butadiynyl complexes.[18]

2. Crystal Structure of 9. No structural data for any type of heterobimetallic C_4 complex have been reported to date.[16] Accordingly, the crystal structure of **9**·CH_2Cl_2 was determined as outlined in Table 3 and the Experimental Section. The molecular structure is shown in Figure 1. Key distances and angles are given in Table 4, and key data for related compounds

Table 2. IR Data for **9**^{n} *n*PF_6^- and Related Compounds

compd	medium	$\nu_{C\equiv C}$ (cm^{-1})	ν_{NO} (cm^{-1})
9	KBr/Nujol	2093 (sh), 2058 (m), 1955 (m)	1622 (vs)
	CH_2Cl_2	2095 (sh), 2058 (m), 1956 (m)	1620 (vs)
9$^+$ PF_6^-	KBr/Nujol	2002 (vs), 1933 (vs), 1876 (m)	1635 (vs)
	CH_2Cl_2	2005 (sh), 1950 (vs), 1882 (m)	1660 (vs)
9^{2+} 2PF_6^-	KBr/Nujol	1941 (vw), 1849 (vw), 1783 (vw)	1701 (vs)
	CH_2Cl_2	1949 (vw), 1851 (vw), 1787 (vw)	1720 (vs)
10	KBr/Nujol	2119 (m), 2097 (m)	1648 (vs)
	CH_2Cl_2	2118 (m), 2098 (m)	1653 (vs)
11	KBr	2113 (s), 1975 (w)	1645 (vs)
	CH_2Cl_2	2115 (s), 1975 (w)	1644 (vs)
13	KBr/Nujol	2165 (m), 2090 (vs), 1980 (s)	
	CH_2Cl_2	2162 (m), 2081 (vs), 1977 (s)	
1a	KBr	1968 (w)	1629 (s)
	CH_2Cl_2	1964 (w)	1623 (s)
1a$^+$ PF_6^-	KBr	1870 (m)	1654 (br)
	CH_2Cl_2	1872 (m)	1665 (s)
1a^{2+} 2PF_6^-	KBr	not obsd	1692 (s, br)
	CH_2Cl_2	not obsd	1719 (s)
1b	CH_2Cl_2	1955, 1880	
1b$^+$ PF_6^-	CH_2Cl_2	1973, 1880	
1b^{2+} 2PF_6^-	CH_2Cl_2	1950, 2160	

Table 3. Crystallographic Data for **9**·CH_2Cl_2

molecular formula	$C_{68}H_{69}FeNOP_3Re$·CH_2Cl_2
molecular weight	1336.13
crystal system	triclinic
space group	$P\bar{1}$
cell dimensions	
a, Å	14.760(8)
b, Å	15.030(2)
c, Å	16.243(6)
α, deg	104.26(4)
β, deg	98.15(6)
γ, edg	111.73(6)
V, Å^3	3134(2)
Z	2
d_{calc}, g/cm^3 (294 K)	1.416
absorption coef. (mm^{-1})	2.366
F(000)	1360
crystal dimensions (mm^3)	0.35 × 0.35 × 0.45
diffractometer	CAD4 NONIUS
radiation (Å)	Mo Kα (0.70926)
data collection method	*ω*/2*θ*
t_{max}/measure, s	60
range/indices (*hk*,*l*)	0, 15; −17, 16; −19,19
θ range	1.34−24.97
decay of standards (25), %	1.2
no. of reflns measd	11043
no. of independent reflns	10573
no. of obsd data, $I > 2\sigma(I)$	8499
no. of variables	689
R_{int} (from merging equiv. reflns)	0.0280
final *R*	0.0412 [R_w = 0.1208]
R indices (all data)	0.0647 [R_w = 0.1317]
GOF	0.991
largest diff peak and hole, e Å^{-3}	1.746 and −1.347

are summarized in Table 5. General features, such as the formally octahedral geometry at each metal, are in accord with past structures in this series.[11,12] Although **9** is somewhat more distorted than homometallic butadiynediyl analogues, most bond lengths and angles fall into previously established ranges (Table 5). As expected, the Fe−C≡ bond (1.895 Å) is shorter than the Re−C≡ bond (2.029 Å), and both are shorter than in model compounds with metal−C(sp^3) bonds (Fe−C = 2.003−2.154 Å and Re−C = 2.123 Å).[24]

(20) Weyland, T.; Lapinte, C.; Frapper, G.; Calhorda, M. J.; Halet, J.-F.; Toupet, L. *Organometallics* **1997**, *16*, 2024−2031.

(21) Roger, C.; Hamon, P.; Toupet, L.; Rabaâ, H.; Saillard, J.-Y.; Hamon, J.-R.; Lapinte, C. *Organometallics* **1991**, *10*, 1045−1054.

(22) These signals were not detectable at room temperature unless spectra were recorded in the presence of a reducing agent (e.g., Na/toluene). Under these conditions **9** slowly decomposes, but the dppe phosphorus atoms give a second-order AA′ pattern with a $^2J_{pp}$ value of ca. 8 Hz.

(23) Interestingly, the ν_{CO} bands in **3a**,**b** are analogously shifted relative to monoiron counterparts (7−10 cm^{-1}), see ref 18.

(24) (a) Roger, C.; Toupet, L.; Lapinte, C. *J. Chem. Soc., Chem. Commun.* **1989**, 713. (b) Hill, D. H.; Parvez, M. A.; Sen, A. *J. Am. Chem. Soc.* **1994**, *116*, 2889−2901. For (η^5-C_5H_5)(η^2-dppe)Fe($CH_2C_6H_5$): (c) Le Bras, J.; Jiao, H.; Meyer, W. E.; Hampel, F.; Gladysz, J. A. For (η^5-C_5Me_5)Re(NO)(P(4-$C_6H_4CH_3)_3$)(CH_3). *J. Organomet. Chem.* **2000**, in press.

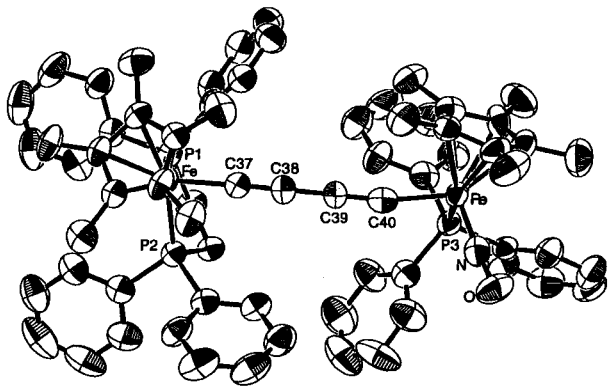

Figure 1. Molecular structure of **9**.

Table 4. Key Distances (Å) and Angles (deg) for **9**·CH_2Cl_2

Fe−P1	2.1628(19)	P1−Fe−P2	86.19(8)
Fe−P2	2.187(2)	P1−Fe−C37	88.49(19)
Fe−C37	1.895(6)	P2−Fe−C37	81.1(2)
Re−P3	2.353(2)	Fe−C37−C38	176.6(5)
Re−C40	2.029(6)		
Re−N1	1.752(6)	N1−Re−P3	93.60(19)
N1−O1	1.212(8)	P3−Re−C40	83.03(18)
C37−C38	1.209(8)	N1−Re−C40	103.4(3)
C38−C39	1.370(9)	Re−C40−C39	169.6(6)
C39−C40	1.224(9)	Re2−N1−O1	171.8(5)
Fe−$C_5Me_{5(centroid)}$	1.740(5)		
Re−$C_5Me_{5(centroid)}$	1.943(5)	C38−C39−C40	177.4(7)
Fe−Re	7.703	C37−C38−C39	178.3(7)

Figure 1 shows that the ReC_4Fe linkage in **9** deviates somewhat from linearity. The Re−C≡C angle is most acute (169.6°), followed by a larger Fe−C≡C angle (176.6°). Most MC_4M complexes feature bond angles of more than 170° (Table 5), although the radical cation **1b**$^+$ PF_6^- has one M−C≡C angle that is even more distorted (167.0°). Even stronger deformations, attributed to packing forces, have also been observed in two (η^5-C_5Me_5)Re(NO)(PPh_3)((C≡C)$_n$-*p*-tolyl) systems.[25] The unsymmetrical diiron complex **3a** also has one somewhat acute M−C≡C angle (172.0°), and the other more linear (177.8°).[18] This was previously attributed to increased metal-to-ligand (d to π^*) back-bonding from the more electron-rich phosphine-substituted endgroup, leading to some $^+$Fe=C=C=C=C(:$^-$)−Fe character and bending at the carbonyl substituted endgroup. While other factors cannot be discounted, the present data suggest an analogous polarization in **9**, with iron as the electron-rich endgroup.

Despite the moderate bending, the iron−rhenium separation (7.730 Å) is longer than the iron−iron distances in **1b**$^+$ PF_6^-,[12a] **3a**,[18] and **5**,[16b] (7.431, 7.570, and 7.653 Å). As expected, it is shorter than the rhenium−rhenium distance in **1a** (7.828 Å).[11] All of the complexes in Table 5 have one C_5Me_5 ligand on each endgroup. These provide reference points for analyzing conformations about the C_4 ligand. We use the centroids to define a twist angle (γ), with 180° and 0° corresponding to anti and syn arrangements. That of **9** (48.3°, Table 5) is the smallest found to date.

3. Cyclic Voltammetry of 9. As illustrated in Figure 2, cyclic voltammograms of **9** show two chemically reversible oxidations, separated by 0.73 V, corresponding to the radical cation **9**$^+$ X^- and dication **9**$^{2+}$ $2X^-$, respectively. A third oxidation, attributed to the trication **9**$^{3+}$ $3X^-$, is observed next to the solvent edge (1.33 V). Such trications have been isolated with some diiron C_4 systems.[14b] Cyclic voltammograms of the related monometallic rhenium (**10**) and iron (**13**) complexes were measured under identical conditions. These gave only one oxidation, which was poorly reversible with rhenium. The iron complex was thermodynamically easier to oxidize ($E°$(**10**−**13**) = 0.35 V). Data are summarized in Table 6.

The $E°$ values (Table 6) require strong interactions between the endgroups. Specifically, substitution of the trimethylsilyl endgroup in the iron complex **13** by the rhenium endgroup renders oxidation 0.50 V more favorable. In accord with the trend for **10** and **13**, oxidation is presumed to have dominant iron character. The second oxidation, which should have more rhenium character, is 0.12 V more favorable than that of **10**. In accord with other observations involving the (η^5-C_5Me_5)Fe(η^2-dppe) fragment, this indicates that even the monooxidized form can behave as an apparent electron-releasing group that facilitates oxidation.[26]

Comparison of the $E°$ values of **9** with those of **1a** and **1b** further supports these conclusions. The oxidation of the iron center in **9** is 0.19 V more difficult than that in **1b**. This suggests that replacement of one of the iron endgroups in **1b** by a rhenium endgroup decreases the electron density at iron. However, the relative magnitudes of the resonance energies associated with the mixed-valence radical cations (which as discussed below should be much greater for the diiron species **1b**$^+$ X^-) constitutes another thermodynamic influence. Similarly, the second oxidation of **9** (i.e., the oxidation of **9**$^+$ X^-) is 0.31 V more facile than the second oxidation of **1a** (i.e., the oxidation of **1a**$^+$ X^-). Thus, from every oxidation state perspective, the iron fragment (η^5-C_5Me_5)Fe(η^2-dppe) is more electron releasing than the rhenium fragment (η^5-C_5Me_5)Re(NO)(PPh_3).[26] This is also in accord with the Mössbauer data for **9** discussed below.

Finally, note that the second oxidation of **9** is 0.12 V more favorable than the first one of **10**. Such behavior, known for **1a**,**b** and **3a**,**b**, indicates that the second metal helps in stabilizing the radical cation. This can be considered as direct evidence for electronic delocalization/interaction along the butadiynediyl bridge in the radical cation. Despite a decreased difference between the two oxidation potentials (0.73 V vs 1.10 or 1.21 V for **3a** and **3b**, respectively), on the whole the cyclic voltammetry of **9** is reminiscent of that for nonsymmetric diiron complexes **3a**,**b**, the main difference being now the chemical reversibility of the second redox process. As we will see in the following section, the double-oxidized state is stable and isolable.

4. Synthesis of 9$^+$ **PF_6^- and 9**$^{2+}$ **$2PF_6^-$.** As shown in Scheme 2, [(η^5-C_5H_5)$_2$Fe]$^+$ PF_6^- (0.95 equiv) and **9** were reacted in CH_2Cl_2. The red solution instantly turned brown. Workup gave the greenish-brown mixed valence (MV) radical cation **9**$^+$ PF_6^- in 86% yield. Similar reactions of **9**$^+$ PF_6^- and [(η^5-C_5H_5)$_2$-Fe]$^+$ PF_6^-, or **9** and excess [(η^5-C_5H_5)$_2$Fe]$^+$ PF_6^-, gave the dication **9**$^{2+}$ $2PF_6^-$ in 98% yield. A correct microanalysis was obtained for **9**$^+$ PF_6^-, and **9**$^{2+}$ $2PF_6^-$ gave a reasonable C/H/N ratio. IR data for both compounds are given in Table 2, and other characterization is detailed below. As expected, **9**$^+$ PF_6^- and **9**$^{2+}$ $2PF_6^-$ gave identical cyclic voltammetry data.

The IR $\nu_{C\equiv C}$ bands of the radical cation **9**$^+$ PF_6^- were at much lower frequencies than those of **9** (ca. 125 cm^{-1}). This indicates a reduced bond order in the carbon bridge in the mixed valence state, consistent with an increased contribution of "cumulenoid" or other resonance structures with reduced triple bond character.

(25) Dembinski, R.; Lis, T.; Szafert, S.; Mayne, C. L.; Bartik, T.; Gladysz, J. A. *J. Organomet. Chem.* **1999**, *578*, 229−246.

(26) Solvation energies also affect $E°$ values. Comparisons of the electron-releasing abilities of the metal endgroups are valid only if the relative solvation energies of the various oxidation states of **1a**, **1b**, **3a**,**b**, **9**, **10**, and **13** do not differ significantly.

Table 5. Selected Crystallographic Reference Data

compd	M1−M2	γ [a]	C≡C	≡C−C≡	M−C≡	M−C≡C	ref
9	7.730	48.3	1.209/Fe	1.370	1.895/Fe	176.6/Fe	this work
			1.224/Re		2.029/Re	169.6/Re	
1a	7.828	107.6	1.202	1.389	2.037	174.45	11
1b$^+$ PF_6^-	7.431	180.0	1.236	1.36	1.830	167.0	12a
3a	7.570	115.4	1.24[b]	1.36	1.90[b]	172.0 [b]	18
			1.21[c]		1.886[c]	177.8 [c]	
4^{3+} $3PF_6^-$	7.411	180.0	1.27	1.33	1.79	175.2	14b
5	7.653	180.0	1.197	1.396	1.933	178.0	16b

[a] Twist angle (γ), $C_5Me_{5(centroid)}-M(1)-M(2)-C_5Me_{5(centroid)}$. [b] At the ($\eta^5$-$C_5Me_5$)(CO)$_2$Fe terminus. [c] At the (η^5-C_5Me_5)Fe(η^2-dppe) terminus.

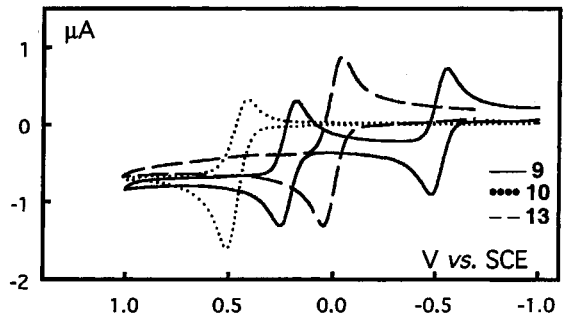

Figure 2. Cyclic voltammograms of **9** and related monometallic complexes (**10**, **13**) in 0.1 M *n*-Bu_4N^+ PF_6^-/CH_2Cl_2 (Pt electrode; V vs SCE; scan rate 0.100 V/s; 20 °C).

Table 6. Electrochemical Data

compd	ΔEp (V)	$E°$ (V)[a]	i_c/i_a	$\Delta E°$ (V)	ref
1a	0.09	+0.01	1	0.53	11
	0.09	+0.54	1		
1b	0.06	−0.69	1	0.72	12a
	0.06	+0.03	1	0.92	
	0.06	+0.95	1		
9	0.07	−0.50	1	0.73	this work
	0.07	+0.23	1	1.92	
	0.07	+1.33	*b*	1.10	
10	0.25	+0.35	3		this work
13	0.09	0.00	1		18

[a] 0.1 M *n*-Bu_4N^+ PF_6^-/CH_2Cl_2 at 20 °C; Pt electrode; scan rate 100 mV/s; V vs SCE; $E°$(ferrocene) = 0.46 V. [b] Ratio difficult to determine with precision due to its position in the solvent diffusion edge.

Similar trends are found with **1a** and **3a**,**b**.[11,18] In contrast, the ν_{NO} band shifts to higher frequency. The magnitude differs somewhat in CH_2Cl_2 solution (40 cm^{-1}) vs KBr or Nujol (13 cm^{-1}). Regardless, this indicates reduced back-bonding into the nitrosyl ligand, consistent with increased positive charge at rhenium. However, these shifts are less than those with **1a** and **1a**$^+$ PF_6^- (CH_2Cl_2, 42 cm^{-1}; KBr, 25 cm^{-1}),[11] where each rhenium in the product carries a formal half charge. This is in accord with greater iron character in the oxidation of **9**, and positive charge density in the resulting radical cation.

For similar reasons, the ν_{NO} band shifts to still higher frequencies upon oxidation of **9**$^+$ PF_6^- to the dication **9**$^{2+}$ $2PF_6^-$ (CH_2Cl_2, 60 cm^{-1}; KBr or Nujol, 66 cm^{-1}). Somewhat smaller shifts are found between **1a**$^+$ PF_6^- and **1a**$^{2+}$ $2PF_6^-$ (CH_2Cl_2, 54 cm^{-1}; KBr, 38 cm^{-1}). The ν_{NO} values for dications **9**$^{2+}$ $2PF_6^-$ and **1a**$^{2+}$ $2PF_6^-$ are quite close, consistent with similar positive charge density on rhenium. In addition, **9**$^{2+}$ $2PF_6^-$ exhibits three very weak bands between 1950 and 1870 cm^{-1}. Although these are in the region of cumulenic absorptions, we hesitate to use them as structural evidence due to their weakness. No comparable IR-active bands were found for **1a**$^{2+}$ $2PF_6^-$ (only a strong Raman absorption at 1883 cm^{-1} in CH_2Cl_2).

The ^{1}H NMR spectrum of **9**$^{2+}$ $2PF_6^-$ at ambient temperature (Table 1 and Experimental Section) shows C_5Me_5 signals very close to those of **9**, **1a**,**b**, and **1a**$^{2+}$ $2PF_6^-$. As expected, the signal for the iron ligand is very different from that of paramagnetic **1b**$^{2+}$ $2PF_6^-$, which is shifted significantly upfield (−6.03 ppm). The PF_6^- ^{31}P NMR signal appeared as a sharp sextuplet, as expected. However, the phosphine ligand signals could not be detected, even after prolonged accumulation times. This could be due to the proximity of the phosphorus nuclei to paramagnetic metal centers. Indeed, the ^{31}P NMR signals are generally not observed in the [(η^5-C_5Me_5)(η^2-dppe)Fe(III)L] and other organometallic series.[27] Under these circumstances, acquisition of the ^{13}C NMR spectrum was not attempted.

Scheme 2. Synthesis of the Consanguineous Complexes **9**$^+$ PF_6- and **9**$^{2+}$ $2PF_6-$

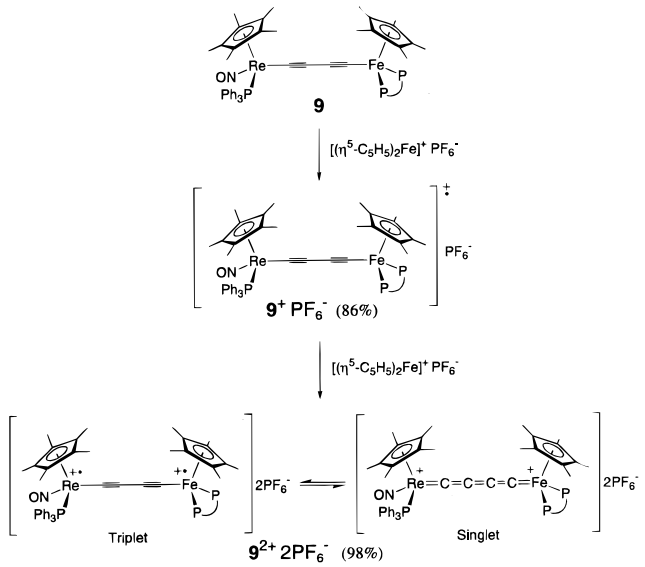

5. ^{57}Fe Mössbauer Data. Mössbauer spectroscopy is a very sensitive probe for identifying the iron oxidation state in adducts of (η^5-C_5Me_5)Fe(η^2-dppe).[28] In addition, quadrupole splittings (QS or ΔE_Q) and isomer shifts can provide insight into the nature of the bonds to iron. Accordingly, ^{57}Fe Mössbauer spectra of the consanguineous series **9**$^{n+}$ nPF_6^- were measured, and data are summarized in Table 7.

At zero field and 80 K, the neutral complex **9** gives a doublet typical of a pure iron(II) system (1.983 mm/s).[28] The QS value does not change significantly with temperature. The slightly increased isomer shift at 80 K compared to that of monoiron complex **13** (0.255 vs 0.245 mm/s)[18] can be attributed to increased electron density at iron due to substitution of the silyl endgroup by the much more electron-rich rhenium. This again shows that there is effective electronic communication between the remote ends of the butadiynediyl spacer. Interestingly, the

(27) Fettinger, J. C.; Mattamana, S. P.; Poli, R.; Rogers, R. D. *Organometallics* **1996**, *15*, 4211−4222.
(28) Guillaume, V.; Thominot, P.; Coat, F.; Mari, A.; Lapinte, C. *J. Organomet. Chem.* **1998**, *565*, 75−80.

Table 7. ^{57}Fe Mössbauer Fitting Parameters

compd	T (K)	δ (mm/s)	QS (mm/s)	Γ (mm/s)	% area
9	80.0	0.255	1.983	0.130	100
	293.0	0.182	1.976	0.116	100
$\mathbf{9}^+ PF_6^-$	4.5	0.197	0.988	0.167	100
	80.0	0.191	0.995	0.194	100
	140.0	0.180	0.975	0.193	100
	210.0	0.156	0.978	0.200	100
	293.0	0.116	0.973	0.202	100
$\mathbf{9}^{2+} 2PF_6^-$	4.5	0.196	0.988	0.167	100
	80.0	0.138	0.957	0.146	100
	293.0	0.053	0.906	0.164	100

isomer shift, more pronounced in **1b** (0.27 mm/s),[12a] confirms that (η^5-C_5Me_5)Fe(η^2-dppe) is more electron releasing than (η^5-C_5Me_5)Re(PPh_3)(NO), in accord with other data above.

The QS value of the mixed-valence complex $\mathbf{9}^+ PF_6^-$ is reduced relative to **9** (0.995 vs 1.983 mm/s, 80 K). This is characteristic of a 17-valence-electron center, and unambiguously indicates that the iron center is best represented by the oxidation state (III).[28] The decreased isomer shift (0.191 mm/s, 80K) relative to **9** is similar to that of the diiron analogues **1b** and $\mathbf{1b}^+ PF_6^-$ ($\Delta IS = 0.06$ mm/s) at 77 K.[12a] Finally, the decreased isomer shift of $\mathbf{9}^{2+} 2PF_6^-$ relative to $\mathbf{9}^+ PF_6^-$ (0.138 vs 0.191 mm/s, 80 K) is suggestive of a further decrease in electron density around iron, consistent with the trend for $\mathbf{1b}^{2+} 2PF_6^-$ ($\Delta IS = 0.03$ mm/s).[12a] The QS value of $\mathbf{9}^{2+} 2PF_6^-$ (80 K) is comparable to that of $\mathbf{9}^+ PF_6^-$ and smaller than that of $\mathbf{1b}^{2+} 2PF_6^-$ (1.32, 77 K).[12a]

Furthermore, the QS value of $\mathbf{9}^{2+} 2PF_6^-$ changes significantly with temperature from 4.5 to 293 K ($\Delta QS = 0.082$ mm/s). This may be indicative of oxidation state and bonding changes, and therefore bridge or spin isomers,[12b] such as the singlet cumulenic and triplet butadiynediyl forms of $\mathbf{1b}^{2+} 2PF_6^-$ (**I**, **II**) described above. However, the presence of only one doublet suggests that if two isomers are simultaneously present, their exchange should be sufficiently fast to give an averaged signal on the Mössbauer time scale (ca. 10^{-8} s).[29a] The splitting trend suggests that the butadiynediyl bridge is relatively more important at higher temperature, and the cumulenic bridge is relatively more important at lower temperature. However, the limiting QS value for a purely cumulenic ReC_4Fe structure is unknown, and might differ significantly from those of purely cumulenic FeC_4Fe structures.[29b] Hence, the equilibrium ratio cannot be assessed.

6. ESR and Magnetism. The ESR spectrum of the radical cation $\mathbf{9}^+ PF_6^-$ was recorded at 293 K in $CH_2Cl_2/ClCH_2CH_2Cl$ (1:1 v/v). As shown in Figure 3a (top), an isotropic and strongly coupled signal ($g_{iso} = 2.0346$) was observed. The coupling of the unpaired electron to rhenium, which can be approximated as a simple nuclear spin 5/2 system, is immediately apparent in the six-line pattern. The dominant isotope of iron (^{56}Fe, 98%) has no nuclear spin. The spectrum was simulated with a line-broadening factor of 48 G. This gave an $A_{iso,Re}$ value of 65 G, two-thirds that of the fully delocalized dirhenium radical $\mathbf{1a}^+ PF_6^-$ (98 G),[11] and one-third those of monorhenium radicals such as $[(\eta^5\text{-}C_5Me_5)Re(NO)(PPh_3)(CH_3)]^+ PF_6^-$ (195−190 G).[17,24b,30,31] This indicates a substantial diminution of spin density on rhenium, consistent with dominant radical character at iron. The $A_{iso,P}$ values were estimated as 12 G for dppe and 36 G for PPh_3. The former compares well with those previously found for (η^5-C_5Me_5)Fe(η^2-dppe)-based radicals.[32]

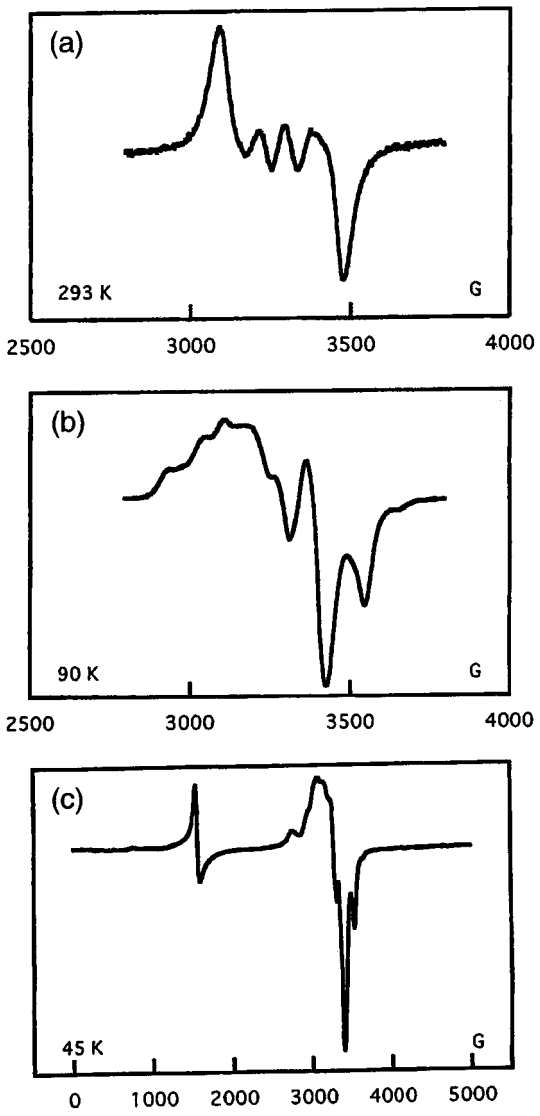

Figure 3. ESR spectra: (a) $\mathbf{9}^+ PF_6^-$ in $CH_2Cl_2/ClCH_2CH_2Cl$ at 293 K; (b) same as spectrum a, but at 90 K glass; and (c) solid sample of $\mathbf{9}^{2+} 2PF_6^-$ at 45 K.

A second spectrum of the same sample was recorded at 90 K in the solvent glass. As shown in Figure 3b (middle), it is more complex due to the presence of three g-tensors, appropriate for a pseudo-octahedral geometry around the radical. The extrapolated values ($g_1 = 1.9202$, $g_2 = 2.0075$, $g_3 = 2.2356$) are typical of an iron-centered radical.[5] The high g_3 tensor value, closer to that for the electron (2.0023) than those of mixed-valence complexes $\mathbf{3a},\mathbf{b}^+ PF_6^-$ ($g_3 = 2.3343$ and 2.3474),[18] suggests that the SOMO in $\mathbf{9}^+ PF_6^-$ is mainly iron-centered and therefore significantly separated in energy from the next lower-lying iron-based molecular orbital.[21] On the other hand, the much higher g_3 value of **13** ($g_3 = 2.4857$) indicates stronger

(29) (a) Guillaume, V.; Mahias, V.; Mari, A.; Lapinte, C. *Organometallics* **2000**, *19*, 1422−1426. (b) Coat, F.; Guillemot, M.; Paul, F.; Lapinte, C. *J. Organomet. Chem.* **1999**, *578*, 76−84.

(30) Meyer, W. E.; Amoroso, A. J.; Jaeger, M.; Le Bras, J.; Wong, W.-T.; Gladysz, J. A. *J. Organomet. Chem.* **2000**, in press.

(31) For ESR measurements of rhenium-centered radicals, see: (a) Klein, A.; Vogler, C.; Kaim, W. *Organometallics* **1996**, *15*, 236−244. (b) Stor, G. J.; van der Vis, M.; Stufkens, D. J.; Oskam, A.; Fraanje, J.; Goubitz, K. *J. Organomet. Chem.* **1994**, *482*, 15−29. (c) Bartley, S. L.; Dunbar, K. R. *Angew. Chem., Int. Ed. Engl.* **1991**, *30*, 448−450; *Angew. Chem.* **1991**, *103*, 447−449. (d) Walker, H. W.; Rattinger, G. B.; Belford, R. L.; Brown, T. L. *Organometallics* **1983**, *2*, 775−776. (e) Baldas, J.; Boas, J. F.; Bonnyman, J.; Pilbrow, J. R.; Williams, G. A. *J. Am. Chem. Soc.* **1985**, *107*, 1886−1891.

(32) Connelly, N. G.; Gamasa, M. P.; Gimeno, J.; Lapinte, C.; Lastra, E.; Maher, J. P.; Le Narvor, N.; Rieger, A. L.; Rieger, P. H. *J. Chem. Soc., Dalton Trans.* **1993**, 2575−2578.

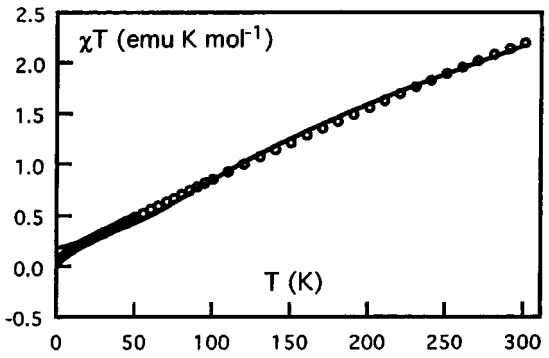

Figure 4. Temperature dependence of the corrected molar magnetic susceptibility χ_m (○) for $\mathbf{9}^{2+}$ $2PF_6^-$. The solid line represents the best fit with eq 1.

interactions between the single electron and electrons of lower-lying orbitals. The higher SOMO/(SOMO-1) energy separation in $\mathbf{9}^+$ PF_6^- relative to $\mathbf{3a,b}^+$ PF_6^- can be attributed to the more electron-rich endgroup, (η^5-C_5Me_5)Re(PPh$_3$)(NO) vs (η^5-C_5Me_5)Fe(CO)$_2$ or (η^5-C_5Ph_5)Fe(CO)$_2$, leading to enhanced repulsive interactions between the two sets of metal-based d orbitals. Thus, the reduced anisotropy of the *g*-tensor ($\Delta g = g_3 - g_1 = 0.3154$) would indicate an increased delocalization of the SOMO relative to $\mathbf{3a,b}^+$ PF_6^-.

Consistent with certain observations above, the dication $\mathbf{9}^{2+}$ $2PF_6^-$ also gave an ESR spectrum. Optimum resolution was achieved with a powdered sample at 45 K (Figure 3c, bottom). The weak signal intensity suggests that the singlet ($S = 0$) state dominates at this temperature. The two distinct patterns in the $\Delta m_s = 1$ and 2 ($g = 4.3046$) regions establish that the ESR active species is a triplet ($S = 1$), consistent with a diradical with two spins. This excludes a variety of impurities or other artifactual sources of the signal. The signal is also broader than that of $\mathbf{9}^+$ PF_6^-. The width of the $\Delta m_s = 1$ signal is similar to that of a diradical with two $S = {}^1/_2$ (η^5-C_5Me_5)(η^2-dppe)Fe(III) centers.[33] The broadening is a consequence of two unpaired electrons on the molecule, which greatly shortens the relaxation time. As the spectrum is not well resolved and the hyperfine structure appears to be complex, determination of the spin Hamiltonian parameters was not straightforward. However, a simulation allows reasonable values for the three *g*-tensor components ($g_1 = 2.04$, $g_2 = 2.10$, $g_3 = 2.15$) and the coupling constants to rhenium ($A_x = 30$ G, $A_y = 50$ G, $A_z = 150$ G) to be extracted.

The spin ground state of $\mathbf{9}^{2+}$ $2PF_6^-$ was further probed on a SQUID magnetometer[34] over the temperature range 5−300 K, using a recrystallized sample. As shown in Figure 4, the molar paramagnetic susceptibility (χ_M) appears to be dominated by intramolecular spin interactions and can be modeled satisfactorily using the modified Bleaney−Bowers expression (eq 1) including the contribution from angular momentum (spin−orbit coupling).[35] Similar treatments are successfully used to evaluate the extent of magnetic exchange between paramagnetic sites in related complexes.[12b,33,36]

$$\chi = (2Ng_{iso}{}^2\mu_B{}^2)(1-\rho)/k_BT[3 + \exp(-J/k_BT)] + (2Ng_{iso}{}^2\mu_B{}^2)\rho/2k_BT + C \quad (1)$$

The line drawn through the points in Figure 4 represents the best fit for the parameters *J*, *C*, and ρ in eq 1. The value calculated for the isotropic constant g_{iso} ($1/3(g_1 + g_2 + g_3)$) is 2.10, and the following values can then be extracted: $J/k_B = -250 \pm 5$ *K* ($J = -175 \pm 4$ cm^{-1}), $C = 0.0050 \pm 0.0002$, $\rho = 0.04 \pm 0.01$. The large negative magnetic exchange coupling constant *J* (-175 cm^{-1}) indicates that $\mathbf{9}^{2+}$ $2PF_6^-$ has a singlet ground state. However, the energy gap between the $S = 0$ and 1 states is sufficiently weak (0.35 kcal/mol) that at ambient temperature the triplet state is appreciably populated (at 300 K: $S/T = 37/63$). This gives credence to the Mössbauer results suggesting two rapidly equilibrating species.[37]

Table 8. UV−Visible and Near-IR Spectral Data (CH_2Cl_2, 280−3000 nm)

compd	$1/D_{Op} - 1/D_S$	λ_{max} (nm)	$10^3\epsilon$ (M^{-1} cm^{-1})
9	0.382	298 (sh)	40.0
		330 (sh)	19.0
		356 (sh)	14.0
$\mathbf{9}^{2+}$ $2PF_6^-$	0.382	410	27.7
		601	28.7
		1087	0.85
$\mathbf{9}^+$ PF_6^-	0.382	296 (sh)	39.0
		374 (sh)	21.0
		388 (sh)	19.0
		448 (sh)	5.0
		868 (sh)	5.7
		1052	34.0
		2500	0.34

7. UV−Visible and NIR Spectra. The UV−visible and near-IR spectra of $\mathbf{9}^{n+}$ $n PF_6^-$ are summarized in Table 8. In general, **9** and $\mathbf{9}^+$ PF_6^- exhibit absorptions similar to those of diiron complexes **3a**,**b** and $\mathbf{3a,b}^+$ PF_6^-.[18] The visible bands of $\mathbf{9}^+$ PF_6^- (448 nm sh; ϵ 5000 M^{-1} cm^{-1}) and $\mathbf{9}^{2+}$ $2PF_6^-$ (410, 601 nm; ϵ 27700, 28700 M^{-1} cm^{-1}) bear a close relationship to those of dirhenium complexes $\mathbf{1a}^+$ PF_6^- (454 nm sh; ϵ 6400 M^{-1} cm^{-1}) and $\mathbf{1a}^{2+}$ $2PF_6^-$ (390, 578 nm; ϵ 39600, 28100 M^{-1} cm^{-1}). Interestingly, the unsymmetrical diiron complex $\mathbf{3a}^+$ PF_6^- gives a very weak intervalence transition in the NIR region (1600 nm; ϵ 360 M^{-1} cm^{-1}). Thus, we sought to check for a similar feature with $\mathbf{9}^+$ PF_6^-.

As shown in Figure 5, $\mathbf{9}^+$ PF_6^- in fact exhibits a very broad and weak NIR band. Unfortunately, solvent absorptions could not be completely subtracted. Regardless, this band is absent in both **9** and $\mathbf{9}^{2+}$ $2PF_6^-$. With $\mathbf{9}^{2+}$ $2PF_6^-$, a weak spin−orbit transition characteristic of the Fe(III) center is also found (2220 nm; ϵ 110 M^{-1} cm^{-1}).[38] The absorption of $\mathbf{9}^+$ PF_6^- was fit to a Gaussian shape, and key parameters were extracted: 2500 nm, ϵ ca. 340 ± 5 M^{-1} cm^{-1},[39] $\Delta\nu_{1/2} = 2150$ cm^{-1}. To check

(33) Weyland, T.; Costuas, K.; Mari, A.; Halet, J.-F.; Lapinte, C. *Organometallics* **1998**, *17*, 5569−5579.

(34) The magnetic moments of **9** and $\mathbf{9}^+$ PF_6^- were measured by the Evans method in CH_2Cl_2. The former was diamagnetic, and the latter gave a value of ca. 1.5 μ_B, close to that for a single unpaired electron (1.73 μ_B): (a) Evans, D. F. *J. Chem. Soc.* **1959**, 2003−2004. (b) Schubert, E. M. *J. Chem. Educ.* **1992**, *69*, 62−62

(35) In this equation, *g* is the isotropic EPR value, μ_B is the Bohr magneton, *N* is Avogadro's number, k_B is the Bolzman constant, and *C* is the positive temperature-independent contribution for the coupling of the ground Kramers doublet with the excited levels through the Zeeman perturbation, see: Kahn, O. *Molecular Magnetism*; VCH: New York, 1993; p 107.

(36) Aquino, M. A. S.; Lee, F. L.; Gabe, E. J.; Bensimon, C.; Greedan, J. E.; Crutchley, R. J. *J. Am. Chem. Soc.* **1992**, *114*, 5130−5140.

(37) This would also explain why the sample, although paramagnetic at room temperature, gives only a slightly shifted ^{1}H NMR spectrum.

(38) This represents a typical LF-metal centered transition of an Fe(III) radical. These are usually observed in fully oxidized iron alkynyl complexes. See: Le Stang, S.; Paul, F.; Lapinte, C. *Inorg. Chim. Acta* **1999**, *291*, 403−425.

(39) It was necessary to use a relatively high concentration of $\mathbf{9}^+$ PF_6^- in our Schlenk cell (ca. 2×10^{-3} M). If the linear domain of the Beer−Lambert law is exceeded, the extinction coefficient can be slightly underestimated.

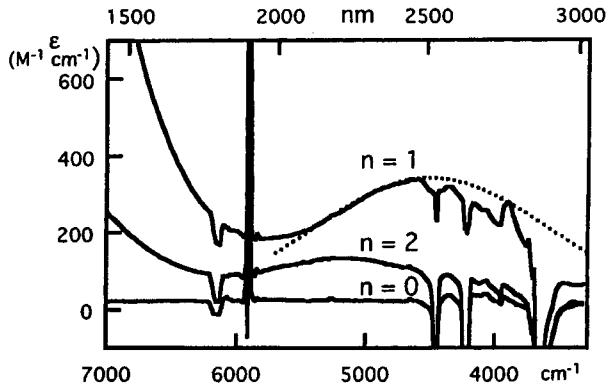

Figure 5. Near/medium IR spectra of $\mathbf{9}^{n+}$ $n\mathrm{PF_6^-}$ in $\mathrm{CH_2Cl_2}$.

Scheme 3. Redox Isomers of $\mathbf{9}^+$ $\mathrm{PF_6^-}$

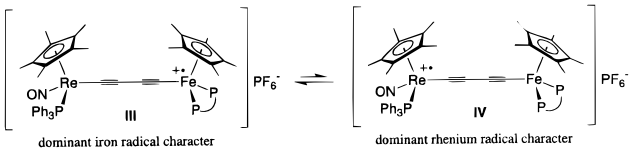

that this transition is not originating from a concentration-dependent ion-pairing mechanism,[40] we verified that its energy was insensitive to the concentration of $\mathbf{9}^+$ $\mathrm{PF_6^-}$. Finally, an analogous band was detected with solid $\mathbf{9}^+$ $\mathrm{PF_6^-}$, but not with solid **9** and $\mathbf{9}^{2+}$ $2\mathrm{PF_6^-}$.

Accordingly, the 2500 nm absorption of $\mathbf{9}^+$ $\mathrm{PF_6^-}$ was assigned to an intervalence transition. In the case of a weakly coupled or type II mixed-valence complex, the Hush model applies.[41,42] The electronic coupling parameter V_{ab} can then be computed in $\mathrm{cm^{-1}}$ using eq 2, where $R_{MM'}$ is the through-space metal−metal distance (Å) and the other terms are as given above. This formula gave a V_{ab} value of 0.021 eV for $\mathbf{3a}^+$ $\mathrm{PF_6^-}$, and yields 0.019 eV (152 $\mathrm{cm^{-1}}$) for $\mathbf{9}^+$ $\mathrm{PF_6^-}$. Both values are quite high for class II complexes.[42] However, much higher values are obtained for class III complexes such as $\mathbf{1a}^+$ $\mathrm{PF_6^-}$ and $\mathbf{1b}^+$ $\mathrm{PF_6^-}$ (0.702−0.620 and 0.47 eV).

$$V_{ab} = 0.0205(\epsilon_{max}\bar{\nu}_{max}\Delta\bar{\nu}_{1/2})^{1/2}/R_{MM'} \qquad (2)$$

Physically, the V_{ab} value of $\mathbf{9}^+$ $\mathrm{PF_6^-}$ represents the electronic coupling of the redox isomers **III** and **IV** in Scheme 3. The former best represents the ground state based upon the many spectroscopic probes above. The free energy difference (ΔG_0) can be approximated by the difference in oxidation potentials between the mononuclear rhenium and iron complexes **10** and **13** in Table 6 (0.36 V or 2904 $\mathrm{cm^{-1}}$). Equation 3 can then be used to calculate the theoretical bandwidth.[5,43] The value obtained is very close to that observed (1916 vs 2150 $\mathrm{cm^{-1}}$). In view of the approximations made and the experimental uncertainty in the numbers, this provides a valuable a posteriori validation of the use of the Hush treatment to extract the electronic coupling value.

$$(\Delta\nu_{1/2})_{theo} = [2300(\bar{\nu}_{max} - \Delta G_0)]^{1/2} \qquad (3)$$

Discussion

The experiments detailed above thoroughly probe the issues summarized in the title of this paper. The synthetic methodology developed earlier for the homobimetallic consanguineous families $\mathbf{1a,b}^{n+}$ $n\mathrm{X^-}$ extrapolates readily to the new conjugal heterobimetallic systems, and needs no further comment. However, every physical probe of structure and electronic ground state presents new issues. In particular, strong electronic communication between the iron and rhenium endgroups is evident in all oxidation states of $\mathbf{9}^{n+}$ $n\mathrm{PF_6^-}$. As noted above, Bruce and Berke have described related series of consanguineous diruthenium and dimanganese C_4 complexes derived from **7** and **8**.[13d,16a] However, a detailed discussion of these interesting homobimetallic systems is beyond the scope of this paper.

The iron and rhenium atoms in neutral complex **9** have 18-valence-electron coordination spheres. As analyzed above, iron/rhenium communication is best reflected in the IR, electrochemical, and Mössbauer data (Tables 2, 6, and 7)—probes that apply to other oxidation states as well. To a first approximation, the interactions can be viewed as classical substituent effects through unsaturated linking groups. For example, the data show that the rhenium fragment (η^5-C_5Me_5)Re(NO)(PPh_3) is less electron releasing than the iron fragment (η^5-C_5Me_5)Fe(η^2-dppe),[12a] but more electron releasing than the carbonyl-substituted fragments (η^5-C_5R_5)$Fe(CO)_2$ (R = Me, Ph).[18] However, we are not aware of any prior systematic studies of heterosubstituted polyynediyl systems. A recent paper offers additional detailed comparisons of IR, NMR, UV−visible, and electrochemical properties of the dirhenium complex **1a**, higher homologues with up to 20 carbons, and mononuclear models (η^5-C_5Me_5)Re(NO)(PPh_3)((C≡C)$_n$X) (n = 2−6).[15]

The radical cation $\mathbf{9}^+$ $\mathrm{PF_6^-}$ is formally derived from one metal with an 18-valence-electron coordination sphere, and another with a 17-valence-electron coordination sphere. Here, the degree of electronic communication is most easily quantified, aided by the extensive literature on other mixed-valence compounds.[41−43] First, the IR, electrochemical, and Mössbauer data show that the radical has dominant iron character, as depicted by **III** in Scheme 3. However, the ESR spectra (Figure 3) show that substantial coupling to rhenium remains, indicative of some ground-state delocalization. The near-IR transition represents, in the context of mixed-valence compounds, a photoinduced electron transfer from iron to rhenium—in other words, an excited state **IV**, with dominant radical character on rhenium. These data also confirm the locus of the electronic hole on the more electron rich termini in the conjugal diiron complexes $\mathbf{3a,b}^+$ $\mathrm{PF_6^-}$.[18]

The metal/metal electronic coupling in $\mathbf{9}^+$ $\mathrm{PF_6^-}$, calculated from the Hush model and eq 2 (V_{ab} = 0.019 eV), is comparable to that of $\mathbf{3a}^+$ $\mathrm{PF_6^-}$ (0.021 eV), but smaller than those of other homometallic class II complexes, e.g., diruthenium(II,III) complexes bridged by 4,4′-bipyridine (0.057 eV), isonicotinato (0.037 eV), and isonicotonamido (0.063 eV) ligands.[44] Equation 2 has been widely applied,[45] but there are potential complications with the resulting V_{ab} values, as recently summarized by Nelsen.[46] Our data provide several cross-checks that appear to validate the Hush treatment, but further work is underway to better define and interpret these energetic parameters.

(40) Goldsby, K. A.; Meyer, T. J. *Inorg. Chem.* **1984**, *23*, 3002−3010.
(41) (a) Hush, N. S. *Prog. Inorg. Chem.* **1967**, *8*, 347−389. (b) Hush, N. S. *Prog. Inorg. Chem.* **1967**, *8*, 391−444.
(42) Robin, M. B.; Day, P. *Adv. Inorg. Chem. Radiochem.* **1967**, 247−422. The class I/II/III categories of mixed-valence complexes signify that the odd electron is (I) localized on one metal, (II) predominantly localized on one metal, but that the complex has an energetically accessible state whereby the electron becomes predominantly localized on the other metal, and (III) fully delocalized over both metals.
(43) Crutchley, R. J. *Adv. Inorg. Chem.* **1994**, *41*, 273−325.
(44) (a) Reimers, J. R.; Hush, N. S. *Inorg. Chem.* **1990**, *29*, 4510−4513. (b) Chou, M. H.; Creutz, C.; Sutin, N. *Inorg. Chem.* **1992**, *31*, 2318−2327.
(45) Patoux, C.; Launay, J.-P.; Beley, M.; Chodorowski-Kimmes, S.; Collin, J. P.; James, S.; Sauvage, J. P. *J. Am. Chem. Soc.* **1998**, *120*, 3717−3725.
(46) Nelsen, S. F. *Chem. Eur. J.* **2000**, *6*, 581−588

The degree of iron/rhenium communication in the dication $\mathbf{9}^{2+}$ $2PF_6^-$ determines the electronic ground state. As shown in Scheme 2 (bottom), there are two possible limiting structures. One features 17-valence-electrons in each metal coordination sphere and a butadiynediyl bridge (triplet), and the other 18-valence-electrons and a cumulenic bridge (singlet). Alternatively said, an anti-ferromagnetic coupling of the odd electrons gives a singlet ground state, and ferromagnetic coupling gives a triplet ground state. Our present data are best interpreted in the context of a temperature-dependent spin equilibrium between singlet and triplet isomers, with the former more stable under the conditions examined. Here, the magnetism data (Figure 4) are particularly crucial, and the Mössbauer and ESR results provide additional support.

As noted in the Introduction, magnetism and IR data show that the diiron complex $\mathbf{1b}^{2+}$ $2PF_6^-$ has a singlet ground state, but a very low lying thermally populated triplet.[12] Thus, thermally equilibrating singlet and triplet states may prove to be quite common in $L_mM(CC)_nML_m$ systems with suitable endgroups (the ML_m fragment must have 16 or fewer valence electrons, or the cumulenic isomer will violate the 18-electron rule). However, the dirhenium complex $\mathbf{1a}^{2+}$ $2PF_6^-$ is purely cumulenic/singlet in character.[11] Preliminary computational studies confirm a strong dependence of these equilibria upon the endgroup.[47] The singlet state of a model complex for $\mathbf{1a}^{2+}$ is 8.0 kcal/mol below the triplet. On the other hand, the triplet state of a model complex for $\mathbf{1b}^{2+}$ is 1.9 kcal/mol below the singlet. Although the latter energy order does not agree with experiment, the computations provide gas-phase values, and the substantially increased relative stability of the triplet is correctly reproduced. Together, these data demonstrate that not only strong electronic but also magnetic interactions can be conveyed through the C_x ligand, and that the degree of the magnetic interaction is decisive for the singlet/triplet ratio at a given temperature.

In summary, this work shows that conjugal heterobimetallic butadiynediyl complexes give rise to consanguineous redox families with strong electronic communication between the endgroups. In contrast to its homometallic parents $\mathbf{1a}^+$ PF_6^- and $\mathbf{1b}^+$ PF_6^-, the conjugal iron−rhenium radical cation $\mathbf{9}^+$ PF_6^- presents a less delocalized structure and behaves as a class-II Robin and Day system.[42] Thus, despite an apparent polarization of the bridge structure in all redox states, the electronic delocalization is not suppressed. Additionally, the structure of the C_4 ligand in the dication $\mathbf{9}^{2+}$ $2PF_6^-$ proves to be strongly influenced by the magnetic interaction between the endgroups. Also, trends previously reported for the related compounds **3a**,**b** have been further supported and/or confirmed. The reversible redox behavior, polarized electronic structures, capabilities for photoinduced electron transfer, and other properties demonstrated above illustrate the potential for polyynediyl-derived organometallics in nanoscale devices, including components for molecular electronics, molecular magnets, and NLO-active assemblies. Work is currently underway to further explore, define, and elaborate the electronic and magnetic properties of these nonsymmetric conjugal systems through additional measurements, bridge extension, and the construction of tailored bridge microenvironments.

Experimental Section

General Data. All manipulations were carried out under inert atmospheres. Solvents or reagents were used as follows: THF, Et_2O, and pentane, distilled from Na/benzophenone; CH_2Cl_2, distilled from CaH_2 and purged with argon; MeOH, distilled from Mg/I_2 and purged with argon; $ClCH_2CH_2Cl$ (ESR), distilled from P_2O_5 and purged with argon; KF, KPF_6, and 18-crown-6 (Aldrich, >99%, >98%, >99%), opened/stored in a glovebox; $[(\eta^5\text{-}C_5H_5)_2Fe]^+$ PF_6^-, prepared by previously published procedures.[48] NMR, IR, UV−vis, and LSI mass spectra were obtained as described earlier.[11,12a,18] Cyclic voltammograms were recorded as described in Table 6 using a PAR model 263 appartus, a SCE reference electrode, and ferrocene as internal calibrant (0.460 V).[48] X-band ESR spectra were recorded on a Bruker ESP-300E spectrometer. Mössbauer spectra were recorded with a 2.5×10^{-2} C (9.25×10^8 Bq) ^{57}Co source using a symmetric triangular sweep mode.[49] Magnetic susceptibilities were determined with a SQUID instrument in a 0.1 T field (1000 G).[33] Elemental analyses were performed at the Center for Microanalyses of the CNRS at Lyon-Solaise, France. LSIMS analyses were effected at the "Centre Regional de Mesures Physiques de l'Ouest" (C.R.M.P.O., Rennes) on a high-resolution MS/MS ZabSpec TOF Micromass spectrometer (8 kV).

$(\eta^5\text{-}C_5Me_5)Fe(\eta^2\text{-}dppe)(C{\equiv}CC{\equiv}C)(Ph_3P)(ON)Re(\eta^5\text{-}C_5Me_5)$ (9). A Schlenk flask was wrapped with aluminum foil and charged with MeOH/THF (2:1, 30 mL), $(\eta^5\text{-}C_5Me_5)Re(NO)(PPh_3)(C{\equiv}CC{\equiv}CSiMe_3)$ (**10**, 0.160 g, 0.220 mmol),[17] $(\eta^5\text{-}C_5Me_5)Fe(\eta^2\text{-dppe})(Cl)$ (**12**, 0.136 g, 0.218 mmol),[21] KPF_6 (0.050 g, 0.270 mmol), and KF (0.015 g, 0.259 mmol). Then 18-crown-6 (0.105 g, 0.398 mmol) in THF (5 mL) was added with stirring. After 48 h, an orange precipitate formed. The dark green overlayer was decanted,[50] and the remaining solid was washed with MeOH (3 × 5 mL) and pentane (5 mL) and dried by oil pump vacuum. This gave **9** as a moderately sensitive orange powder (0.150 g, 0.119 mmol, 65%). It can be further purified by dissolving in toluene (25 mL), and filtering the concentrated solution through Celite (1−2 cm). Precipitation with pentane affords ca. 95% recovery. Alternatively, deep red cubic shaped crystals of $\mathbf{9}\cdot CH_2Cl_2$ can be grown by slow diffusion of pentane (layer/layer) into a concentrated CH_2Cl_2 solution (0.100 g, 0.079 mmol, 43%).[51] Calcd for $C_{68}H_{69}FeNOP_3Re\cdot CH_2Cl_2$: C, 62.02; H, 5.36; N, 1.05. Found: C, 62.82; H, 5.67; N, 1.14. MS (positive LSI, 3-NBA) 1251 ($\mathbf{9}^+$, 100%), 589 ($(\eta^5\text{-}C_5Me_5)Re(NO)(PPh_3)(C_4)^+$, 20%). NMR ($\delta$, C_6D_6): ^1H (300 MHz) 8.1−7.8, 7.2−7.0 (2m, $7C_6H_5$), 2.69 (br s, 2H of CH_2CH_2), 1.76 (br s, $(C_5(CH_3)_5)Re$, 2H of CH_2CH_2), 1.50 (br s, $(C_5(CH_3)_5)Fe$); $^{13}C\{^1H\}$ (75.5 MHz) 137.8−124.5 (m, PPh_2, PPh_3), 121.3, 106.4, 76.7 (3br s, tentatively assigned to C≡CC≡C), 99.6 (s, $(C_5(CH_3)_5)Re$), 87.5 (s, $(C_5(CH_3)_5)Fe$), 31.2 (br s, CH_2), 10.4 (s, $(C_5(CH_3)_5)Fe$), 10.2 (s, $(C_5(CH_3)_5)Re$); $^{31}P\{^1H\}$ (121 MHz) 102.9 (s, dppe), 20.9 (s, PPh_3). Other spectroscopic data are given in Tables 1, 2, and 6−8.

$[(\eta^5\text{-}C_5Me_5)Fe(\eta^2\text{-}dppe)(C{\equiv}CC{\equiv}C)(Ph_3P)(ON)Re(\eta^5\text{-}C_5Me_5)]^+$ PF_6^- ($\mathbf{9}^+$ PF_6^-). A Schlenk flask was charged with $[(\eta^5\text{-}C_5H_5)_2Fe]^+$ PF_6^- (0.065 g, 0.196 mmol), **9** (0.260 g, 0.208 mmol), and CH_2Cl_2 (15 mL). The solution was stirred for 1.1 h at room temperature and concentrated by oil pump vacuum to ca. 5 mL. Pentane (50 mL) was added. The dark precipitate was decanted, washed with toluene (2 × 3 mL) and pentane (3 × 3 mL), and dried under vacuum to give $\mathbf{9}^+$ PF_6^- as a dark green powder (0.235 g, 0.168 mmol, 86%).[51] Calcd for $C_{68}H_{69}F_6FeNOP_4Re$: C, 58.50; H, 4.98; N, 1.00. Found: C, 58.53; H, 5.09; N, 0.99. Spectroscopic data are given in Tables 1, 2, and 6−8.

$[(\eta^5\text{-}C_5Me_5)Fe(\eta^2\text{-}dppe)(CCCC)(Ph_3P)(ON)Re(\eta^5\text{-}C_5Me_5)]^{2+}$ $2PF_6^-$ ($\mathbf{9}^{2+}$ $2PF_6^-$). A Schlenk flask was charged with $[(\eta^5\text{-}C_5H_5)_2Fe]^+$ PF_6^- (0.057 g, 0.172 mmol), $\mathbf{9}^+$ PF_6 (0.245 g, 0.175 mmol), and CH_2Cl_2 (15 mL). The solution immediately turned deep blue-green and was stirred for 3.5 h at room temperature and concentrated by oil pump vacuum to ca. 5 mL. Pentane (50 mL) was added. The precipitate

(47) Jiao, H.; Gladysz, J. A. Manuscript in preparation. Dications $\mathbf{1a}^{2+}$ and $\mathbf{1b}^{2+}$ were modeled (B3LYP density functional theory) by $[(\eta^5\text{-}C_5H_5)(NO)(PH_3)ReC_4Re(PH_3)(NO)(\eta^5\text{-}C_5H_5)]^{2+}$ and $[(\eta^5\text{-}C_5H_5)(\eta^2\text{-}H_2PCH_2CH_2PH_2)FeC_4Fe(\eta^2\text{-}H_2PCH_2CH_2PH_2)(\eta^5\text{-}C_5H_5)]^{2+}$.

(48) Connelly, N. G.; Geiger, W. E. *Chem. Rev.* **1996**, *96*, 877−910.

(49) Greenwood, N. N. *Mössbauer Spectroscopy*; Chapman and Hall London, 1971.

(50) In the case that no precipitation occurs after 48 h, solvent is removed from the dark green reaction mixture by oil pump vacuum. The dark green residue is extracted with toluene (4 × 5 mL) until the purple extracts become colorless. The toluene is removed by vacuum and the deep purple residue is washed with MeOH (4 × 5 mL, until the purple washings become colorless) and pentane (2 × 3 mL) and dried by oil pump vacuum. The remaining orange solid **9** can then be further purified.

(51) IR data are given in Table 1.

was decanted, washed with Et_2O (2 × 5 mL), and dried under oil pump vacuum to give $\mathbf{9}^{2+}$ $2PF_6^-$ as deep blue-green powder (0.260 g, 0.168 mmol, 98%).[51] ^1H NMR (δ, CD_2Cl_2, 200 MHz) 7.57−6.55 (6m, $7C_6H_5$), 3.8 (br m, 2H of CH_2CH_2), 2.25, 1.20 (2br s, 2H of CH_2CH_2, $(C_5(CH_3)_5)$Re and $(C_5(CH_3)_5)$Fe). Spectroscopic data are given in Tables 1, 2, and 6−8.

Crystallography. Data were collected on a cubic crystal of $\mathbf{9}\cdot CH_2Cl_2$ (above) as summarized in Table 3.[52] Cell constants and an orientation matrix were obtained from a least-squares refinement using 25 high-θ reflections. After Lorentz and polarization corrections[53] and absorption corrections (φ scans),[54] the structure was solved with SIR-97[55] which revealed the non-hydrogen atoms and the CH_2Cl_2 solvate. After anisotropic refinements, a Fourier difference map revealed many hydrogen atoms. The whole structure was next refined by SHELX-93[56] by full-matrix least-squares techniques (use of F squared magnitude; x, y, z, β_{ij} for Re, Fe, P, N, O, and C atoms, and x, y, z in riding mode for H atoms; calc $w = 1/[\sigma^2(F_o^2) + (0.0911P)^2 + 4.5203P]$, where $P = (F_o^2 + 2F_c^2)/3$). Atomic scattering factors were taken from the literature.[57] Ortep views were generated with PLATON-98.[54] All calculations were performed on a Silicon Graphics Indy computer.

Acknowledgment. We thank the Center National de la Recherche Scientifique (CNRS), the US NSF, the Deutsche Forschungsgemeinschaft (DFG, GL 300/2), and NATO for support of this research.

Supporting Information Available: Complete X-ray crystallographic data for complex $\mathbf{9}\cdot CH_2Cl_2$ (PDF). This material is available free of charge via the Internet at http://pubs.acs.org.

JA0011055

(52) Fair, C. K. *MolEN*. An Interactive Intelligent System for Crystal Structure Analysis; ENRAF-NONIUS: Delft, The Netherlands, 1990.

(53) Spek, A. L. *HELENA*. Program for Handling of CAD4-Diffractometer Output SHELX(S/L); Utrecht University: Utrecht, The Netherlands, 1997.

(54) Spek, A. L. *PLATON-98*. A Multipurpose Crystallographic Tool; Utrecht University: Utrecht, The Netherlands, 1998.

(55) Altomare, A.; Burla, M. C.; Camalli, G.; Cascarno, G.; Giacovazzo, C.; Guagliardi, A.; Moliterni, A. G. G.; Polidori, G.; Spagna, R. L. *J. Appl. Cryst*. **1998**, *31*, 74−77.

(56) Sheldrick, G. M. *SHELX-93*. Program for Refinement of Crystal Structures; University of Göttingen: Göttingen, Germany, 1993.

(57) Reidel: D. *International Tables for X-ray Crystallography*; Kynoch Press: Birmingham, 1974; Vol. IV.